

Dynamic Range Compression Deconvolution for Enhancement of Automatic Target Recognition System Performance

Bahareh Haji-saeed¹, Jed Khoury², W. D. Goodhue³, Charles L. Woods² and John Kierstead¹

¹Solid State Scientific Corporation, Hollis, NH 03049

²Air Force Research Laboratory / RYHC, Hanscom Air Force Base, MA 01731

³Physics Department, University of Massachusetts, Lowell, MA, 01854

ABSTRACT

A generic nonlinear dynamic range compression deconvolver (DRCD) is proposed. We have performed the dynamic range compression deconvolution using three forms of nonlinearities: (a) digital implementation- A-law/ μ -law, (b) hybrid digital-optical implementation- two-beam coupling photorefractive holography, and (c) all optical implementation- MEMS deformable mirrors. The performance of image restoration improves as the saturation nonlinearity increases. The DRCD could be used as a preprocessor for enhancing Automatic Target Recognition (ATR) system performance. In imaging through atmosphere, factors such as rain, snow, haze, pollution, etc. affect the received information from a target; therefore the need for correcting these captured images before an ATR system is required. The DRCD outperforms well-established image restoration filters such as the inverse and the Wiener filters.

Keywords: Adaptive Optics; nonlinear optical signal processing; automatic target recognition

1. INTRODUCTION

Imaging in atmospheric turbulence has been a research topic for many years. In atmospheric optics, factors such as rain, snow, sleet, fog, haze, pollution, etc., affect the observed object's image while using any kind of optical system. These factors can also affect the optical wave propagation through the atmosphere thereby distorting and redirecting a portion of the phasefront. Thus, receiving optics is unable to focus the image. These effects produce negative consequences in ATR imaging, remote sensing, laser radar, astronomical imaging, free space optical communication, and any other applications that need optical wave transmission through the atmosphere. In addition, image quality is distorted by permanent manufacturing errors and by long time scale wavefront aberrations introduced by mechanical, thermal, and optical effects in the telescope, such as defocusing, decentering, or mirror deformations generated by their supporting devices¹. However, within the last decade there has been a revolution in ground-based optical and infrared astronomy imaging. The development of "Adaptive Optics (AO)" has demonstrated that the blurring effects of atmospheric turbulence or any kind of optical imperfections can be analyzed and corrected. AO compensates for distortion in the wave propagation such as atmospheric turbulence in real time with captured observations from the object. In principle, very faint objects can be imaged in long exposures with a bright guide star nearby to allow the AO system to analyze the atmospheric effects. With the advantage of having high speed computers, many kinds of computational methods have been developed for restoring images from distortions as well as noise reduction. For instance if either the distortion function or the image function (estimated image function) is known, methods such as Minimum Mean Square Error (Wiener) filter for systems with noise and Inverse filter for systems without noise can recover the other function². However, if the atmospheric turbulence becomes a severe scattering medium, most conventional approaches, such as inverse filtering and Wiener filtering, will not be adequate for correcting the captured images.

To overcome the shortcomings with the conventional image restoration approaches, we propose a dynamic range compression image restoration technique. Dynamic range compression/expansion, known as companding (compressing-expanding), is a well-established principle for recovering signals embedded in high noise. Our group pioneered several optical nonlinear companding schemes for all-optical correlators and image enhancers^{2,3}. In this paper we have extended our prior work to introduce the first dynamic range compression deconvolution. This paper summarizes our proposed techniques in this area. Dynamic range compression, accompanied with conventional image restoration, might be useful in recovering images embedded in a high noise and cluttered environment. Such an approach might overcome even the Wiener filter limitations. This technique can be used for preprocessing captured images before they are sent to ATR systems. High quality images are required for enhancing ATR system performance. Dynamic range compression/expansion nonlinearity, when applied to a noisy signal, improves the signal to noise ratio in areas where the

signal is low compared to the noise and reduces the SNR in areas where the signal is higher than the noise level. This principle has been used to improve the quality of acoustic signals in the 50's and is extensively used for noise reduction in tape recording limited by "tape hiss", which is high frequency random noise. Noise reduction systems like "Dolby" and "dbx" help to solve this problem by pre-emphasizing (compression) the high frequencies before recording onto tape in order to increase their amplitude over tape hiss noise with which they compete. Upon playback, a matched de-emphasis filter (expansion) is employed. These noise reduction systems are amplitude sensitive so that only soft high-frequency sounds are emphasized. The matched de-emphasis filter scales the high frequencies with the other recorded signals⁴. Dynamic Range Compression/Expansion technique has also been used in telecommunication systems using a nonlinear element for simultaneously compressing the data (reducing the signal's dynamic range for uniform quantization process), enhancing the SNR and at the receiver end expanding the data through the inverse of the same nonlinear element^{5,6}.

2. DYNAMIC RANGE COMPRESSION DECONVOLUTION ARCHITECTURE

A generic architecture of dynamic range compression deconvolution is shown in figure 1.

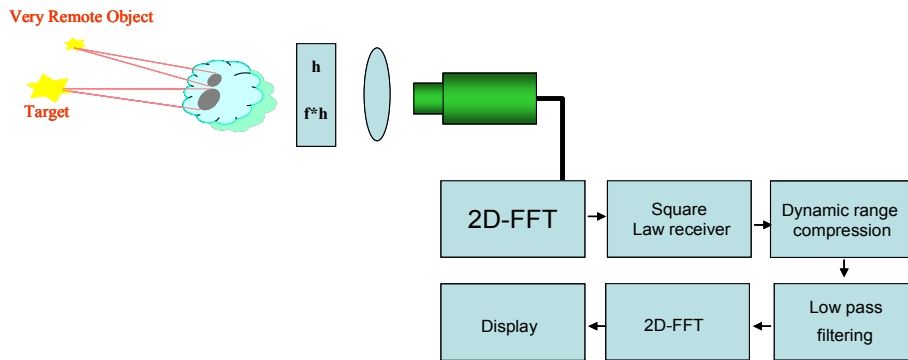


Figure 1. Dynamic range compression deconvolution

A joint image of the target and a remote source, $h+f^*h$, is captured by a CCD camera, where h is the aberration function (blur) impulse response and f^*h is the blurred image. The joint image is Fourier transformed and captured by a square-law receiver which could simply be a CCD camera or a two-beam coupler as demonstrated in the holographic implementation below. The square-law receiver is responsible for mixing the spectra to produce the cross products. The output of the square-law receiver is then sent to the dynamic range compression device. The dynamic range compression deconvolution can be implemented digitally or optically. The output from the dynamic range compression device is then lowpass filtered, Fourier transformed and finally displayed as the recovered image which can be used for ATR systems. In another word, the DRCD pre-process the captured images and recover them from any distortions and noise before they sent to an ATR system.

The output of the square-law receiver is given by:

$$|H + FH|^2 = |H|^2 + |F|^2 |H|^2 + HF^* H^* + H^* FH \quad (1)$$

where H and FH are the Fourier transforms of the blur impulse response, h , and the blurred image, f^*h , respectively. The first term corresponds to the autocorrelation of the aberration impulse response; the second term corresponds to the correlation of the blurred image with itself. The third and the fourth terms correspond to the corrected image and its conjugate from phase distortion, respectively. Correcting the phase distortion; however, will not be sufficient to completely recover images from distortion and noise; therefore, we propose to use dynamic range compression to overcome these limitations. The dynamic range compression saturation nonlinearity performs three functions: (a) Enhances the signal-to-noise ratio (SNR) at high spatial frequencies where SNR is low; (b) Enhances high frequencies relative to low frequencies; and (c) Converts the noise to very high frequency noise. This subsequently spreads noise to be low intensity over a large area in the image plane. The high frequency enhancement relative to low frequencies is an essential function for recovery of high frequency intensity in blurred signals. Consequently this should have a significant effect on SNR in the image plane. The lowpass filtering performs two functions: (a) Recovery of the spatial frequencies

intensities near their expected values (gray level image); and (b) Further enhancement of SNR, since lowpass filters reduce noise.

In contrast to image restoration techniques based on Inverse filtering, and Wiener filtering, the proposed dynamic range compression deconvolution can recover signals embedded in a very high noise environment. Computer simulations predict that the two beam coupling compression deconvolution shown below outperforms image restoration using Wiener filtering. The Wiener filter has been the main filter used for image restoration for over half a century. We have performed the dynamic range compression deconvolution using three forms of nonlinearities: (a) digital implementation- A-law/ μ -law⁷, (b) hybrid digital-optical implementation- two beam coupling photorefractive holography^{8,9}, and (c) all optical implementation- MEMS deformable mirrors¹⁰⁻¹². The performance of image restoration improves as the saturation nonlinearity increases.

3. DYNAMIC RANGE COMPRESSION DECONVOLUTION- A-LAW AND μ -LAW

In this section, dynamic range compression image deconvolution via both the A-law and the μ -law encoders is introduced for the first time⁷. Figure 2 shows the proposed architecture of A-law/ μ -law joint Fourier processor.

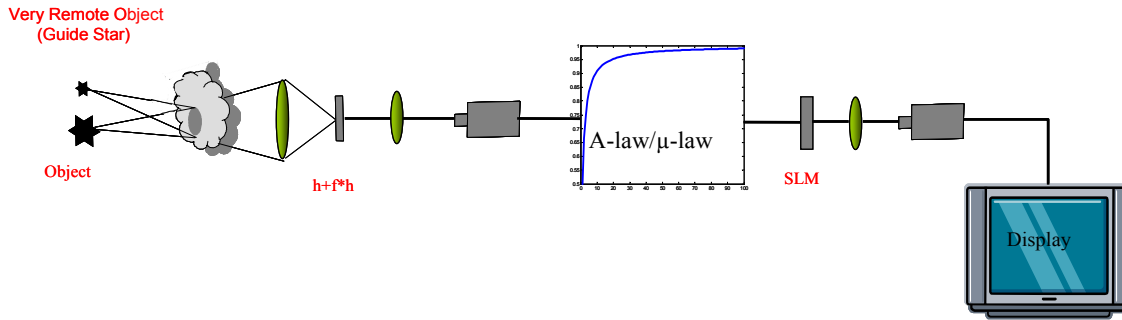


Figure 2. Adaptive Optics imaging system for image restoration using A-law/ μ -law

The reference and the signal information, corresponding to a point source (guide star or multi guide stars) and the object of interest, are passing through the distortion medium which produce $h + f*h$ joint image where “h” is the impulse response of the distortion medium, f is the object, “f*h” is the distorted image and asterisk “*” is the convolution symbol. Then they are jointly Fourier transformed via a lens to a CCD camera which acts as a square-law receiver and is responsible for mixing the spectra to produce the cross products. The output from the CCD camera is sent to the A-law/ μ -law digital or analog receiver. After nonlinear A-law or μ -law dynamic range compression deconvolution the output is sent to a spatial light modulator (SLM), the output from the SLM is then Fourier transformed via a lens to produce the processed output. The output is then lowpass filtered to show the gray level image. As shown in equation 1, the CCD camera is responsible for combining the Fourier transforms of the impulse response and the distorted image to compensate for the phase distortion. And then the A-law/ μ -law nonlinear transformation is responsible for enhancing high frequencies, and hence noise reduction and signal to noise ratio enhancement. The input-output nonlinear transfer functions of the A-law and the μ -law receivers are respectively defined as⁶

$$f(E) = \frac{1 + \ln A |E|}{1 + \ln A} \text{sgn}(E) \quad (2)$$

$$f(E) = \frac{\ln(1 + \mu |E|)}{\ln(1 + \mu)} \text{sgn}(E) \quad (3)$$

Where

$$\text{sgn}(E) = \begin{cases} 1 & \text{for } E \geq 0 \\ -1 & \text{for } E < 0 \end{cases} \quad (4)$$

and E is the input information. In a joint Fourier processor E is always larger than 0 and hence $\text{sgn}(E)$ is always 1. The parameters A and μ controls the amount of compression. In the standard systems $A=87.6$ and $\mu=255$.

Figure 3 shows some of the simulation results. This figure represents the results of deconvolution for the atmospheric turbulence. In this figure, (A) is the noisy blurred input with SNR= 5, (A') and (A'') are the corresponding recovered images via the A-law and the μ -law deconvolutions respectively. The B and C rows are sequentially the same as the A row for SNR=1 and SNR=0.1 respectively.

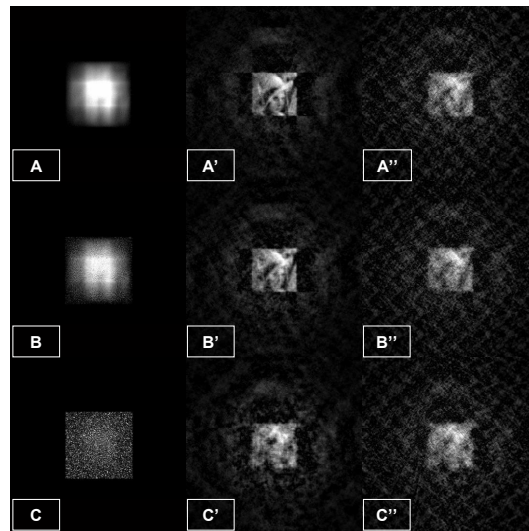


Figure 3. Atmospheric turbulence indirect simulation results (A) the noisy blurred input with SNR= 5, (A') and (A'') are the corresponding recovered images via the A-law and the μ -law deconvolutions respectively. The B and C rows are sequentially the same as the A row for SNR=1 and SNR=0.1 respectively.

Figure 4 represents a comparative study of the A-law deconvolution with both of the Wiener and the Inverse filters. In this figure (A) represents the recovered image via the A-law deconvolution for SNR=1 (the (B') image in figure 10), (B) is the recovered image using the Wiener filter, with the expected value of F, (C) is the recovered image using Inverse filtering and (D) is the recovered image using the Wiener filter, with the exact value of F. As it is evident in C, the Inverse filter was incapable of either recovering or even detecting the image and noise is simply covering the whole array. By comparing the A with the D, it is clear that the image recovery of the noisy blurred signal with SNR=1 via the A-law deconvolution was always better (with a generic shape of the low pass filter or the expected value of F) than the Wiener filter with the exact value of F. When the exact value of F was replaced by a generic shape of the low pass filter or the expected value of F like what was used in the A-law results, the Wiener filter failed as it is evident in B.

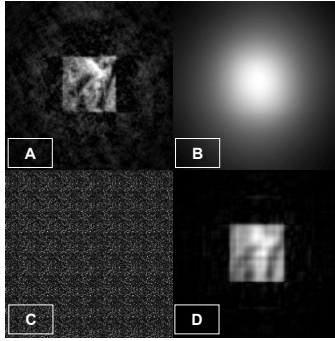


Figure 4. A-law deconvolution result for the atmospheric turbulence compared to Wiener and Inverse filters results (A) the recovered image via the A-law deconvolution for SNR=1, (B) the recovered image using Wiener filter, with the expected value of F, (C) the recovered image using Inverse filtering and (D) is the recovered image using the Wiener filter, with the exact value of F

Both the A-law and the μ -law deconvolutions are associated with noise conversion from low frequencies to high frequencies. This frequency conversion leads to further enhancement of the signal to noise ratio through spreading the noise over the entire array. While in image recovery via the Wiener filter, the noise remains nearly concentrated on the original noisy image area. The A-law and the μ -law encoders are used in both digital and analog systems. The dynamic range compression severity is controlled via the compression parameters A and μ for A-law and the μ -law respectively. The simulation results were improved when these parameters increased; in other words increasing the nonlinear dynamic range compression severity affects the performance in image restoration. Therefore in the next subsequent two sections we will study more severe nonlinearities by focusing on the optical implementation of the first order power-law expansion of the A-law/ μ -law deconvolution which has more nonlinear severity.

4. DYNAMIC RANGE COMPRESSION DECONVOLUTION- TWO-BEAM COUPLING

In this section our hybrid digital-optical implementation of the dynamic range compression deconvolution via a two-beam coupling arrangement is presented^{8,9}. The impulse response of the distorted function and the distorted image are jointly transformed to pump a reference beam in a two-beam coupling setup. The Fourier transform of the pumped reference beam contains the deconvolved image and its conjugate.

Figure 5 shows the proposed architecture of our two-beam coupling joint Fourier processor.

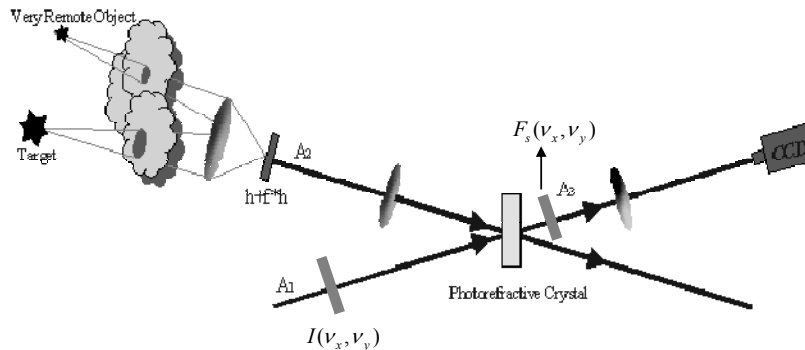


Figure 5. Two-beam coupling joint Fourier processor

A joint image of a remote source and the object is captured via an optically or electrically addressed spatial light modulator for processing. The Fourier transform of the joint image (A_2) is used to pump either a clean or a spectrally

variant reference beam (A_1) via a nonlinear photorefractive element. The CCD camera captures the Fourier transform of the lowpass filtered diffracted beam (A_3). This beam contains gray level information for the corrected image and its conjugate. The spectrally variant reference beam is shaped through a beam profiler. A beam profiler is a SLM addressed by the joint spectra envelope through direct measurement. The beam profiler is essential to reduce extremely high beam ratios required to achieve dynamic range compression. The deflected output from the crystal is spatially filtered through an amplitude lowpass filter $F_s(v_x, v_y)$. The output of this filter is Fourier transformed to produce the joint spectra gray level recovered information and is given by:

$$A(v_x, v_y) = A(0) \left[\frac{1 + m / (\lambda f_l)^2 |R(v_x, v_y) + S(v_x, v_y)|^2}{1 + m / (\lambda f_l)^2 |R(v_x, v_y) + S(v_x, v_y)|^2 \exp(-\Gamma l)} \right]^{1/2} F_s(v_x, v_y) \quad (5)$$

where v_x and v_y are spatial frequencies, m is the beam intensity ratio before passage of the signal beam through the transparency bearing objects, λ is the wavelength, f_l is the focal length, and R and S are H and HF, respectively. According to this equation, the nonlinear transfer function of the diffracted beam consists of square-law receiving and saturation nonlinearity. The saturation nonlinearity is associated with energy transfer of two beam coupling⁸.

For simulating the two beam coupling, similar simulations format as the A-law/ μ -law simulations have been performed, in order to have an easy performance comparison. Figure 6 represent the results of deconvolution for the atmospheric turbulence blur function. In this figure (A) is the noisy blurred input with SNR= 5, (A') and (A'') are the corresponding recovered images via the spectrally invariant and variant deconvolutions respectively. The B and C rows are sequentially the same as the A row for SNR=1 and SNR=0.1 respectively. Figure 7 represents a comparative study of the spectrally variant deconvolution with both of the Wiener and the Inverse filters. In this figure (A) represents the recovered image via the spectrally variant deconvolution for SNR=1 (the (B') image in figure 6), (B) is the recovered image using the Wiener filter, with the expected value of F , (C) is the recovered image using Inverse filtering and (D) is the recovered image using Wiener filter, with the exact value of F .

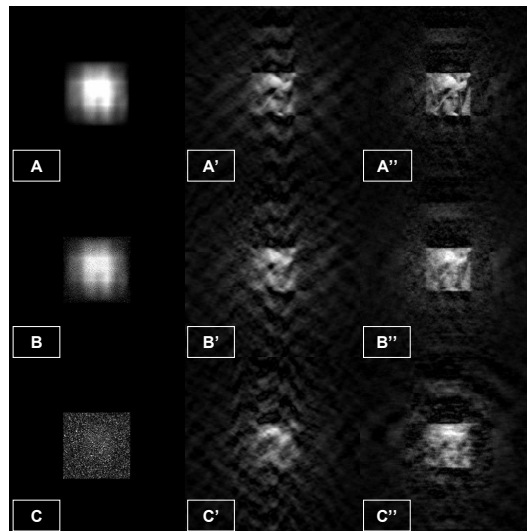


Figure 6. Atmospheric turbulence indirect simulation results (A) is the noisy blurred input with SNR= 5, (A') and (A'') are the corresponding recovered images via the spectrally invariant and variant deconvolutions respectively. The B and C rows are sequentially the same as the A row for SNR=1 and SNR=0.1 respectively.

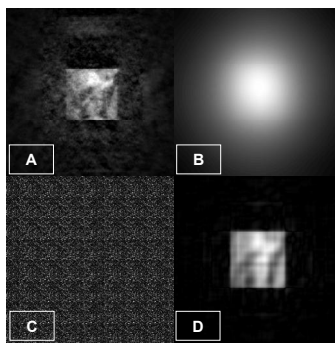


Figure 7. The spectrally variant deconvolution result for the atmospheric turbulence compared to Wiener and Inverse filters result, (A) the recovered image via the spectrally variant deconvolution for SNR=1, (B) the recovered image using Wiener filter, with the expected value of F , (C) the recovered image using Inverse filtering and (D) the recovered image using Wiener filter, with the exact value of F .

5. DYNAMIC RANGE COMPRESSION DECONVOLUTION- OPTICAL LIMITER MEMS

In previous sections, the dynamic range compression A-law/ μ -law and two-beam coupling were demonstrated. The drawback in two-beam coupling deconvolution is that the response time at very high frequencies becomes extremely large (slow in processing speed) since the response time of the photorefractive crystals is inversely related to the total intensity incident on the crystal¹³⁻¹⁵. Other limitation associated with two beam coupling deconvolution is the need for an input spatial light modulator. This may cause some problems in particular for remote sensing where the light is incoherent. The interface between the spatial light modulator and CCD camera imposes other constraints in systems for correcting supersonic turbulence. Therefore one way to overcome this limitation is to use an all-optically addressed spatial light modulator where all the pixels are addressed independently in parallel. Furthermore one can also design an all optically addressed spatial light modulator with dynamic range compression capability.

In this section, the implementation of dynamic range compression deconvolution is proposed using a newly designed Nonlinear Optical Limiter MEMS (NOLMEMS) device^{11,12}. NOLMEMS dynamic range compression has several advantages over two-beam coupling deconvolution: (1) the membrane reflectivity is $\sim 100\%$. This overcomes the problem of the photorefractive crystal's low grating efficiency caused by high beam intensities for achieving the dynamic range compression, (2) the processing time is in μsec scale (dictated by the membrane response time) compared to msec time with two beam coupling (dictated by the photorefractive materials response time), (3) no response time dependency on spatial frequency intensities as in the spectrally variant deconvolution, (4) it approaches the saturation limit faster than the two beam coupling which is more effective in extracting the amplitude information for better image recovery, (5) it can work with both coherent and incoherent light, (6) optical limiter with an optical amplification capability integrated with photodetectors, can have response to broad-band ultra-low light intensities.

Figure 8 shows the proposed nonlinear optical-limiter MEMS device (NOLMEMS). Reference (R) and signal (S) are jointly Fourier transformed by a lens, L, into an all-optically addressed MEMS deformable mirror located at one facet of a cubic beam splitter. Reference and signal correspond to a very remote object and the target passing through the atmosphere, respectively. The deformable mirror functions as an array of parabolic mirrors. The focal point of each of these parabolic mirrors is dependent on the joint spectra back-illumination intensity. The saturation focal plane is located within distance f_s from the deformable mirror. A plane-wave counter to the joint spectra of the images is incident to the front side of the deformable mirror. The plane wave is reflected out of the parabolic micro-mirror to a focused array of wavelets. Depending on the joint spectra back-illumination intensity, each of the wavelets is focused on a different focal plane. The minimum focal length of each of the micro-deformable mirrors is always greater than or equal to f_s . A plano-concave lens is located at the other facet of the beam splitter, imaging the saturation focal plane into an array of pinholes. The pinhole array is aligned to the center of the converging wavelets. Only a portion of the converging wavelets is transmitted through the pinhole array. An array of wavelet sources is generated after transmission within the pinhole array. The array of point sources from the pinhole array is collimated to a plane-wave using a lenslet array. The

superposed wavefront of plane wave arrays from the micro-mirror represents a dynamic range compression version of the joint spectra of the reference and the signal information. The superposed plane wave consists of a collimated wavelet array which is spatially lowpass filtered. After spatial filtering, the output is Fourier transformed by a lens, L, into a CCD camera, thereby producing the required joint Fourier transform signal processing functionality.

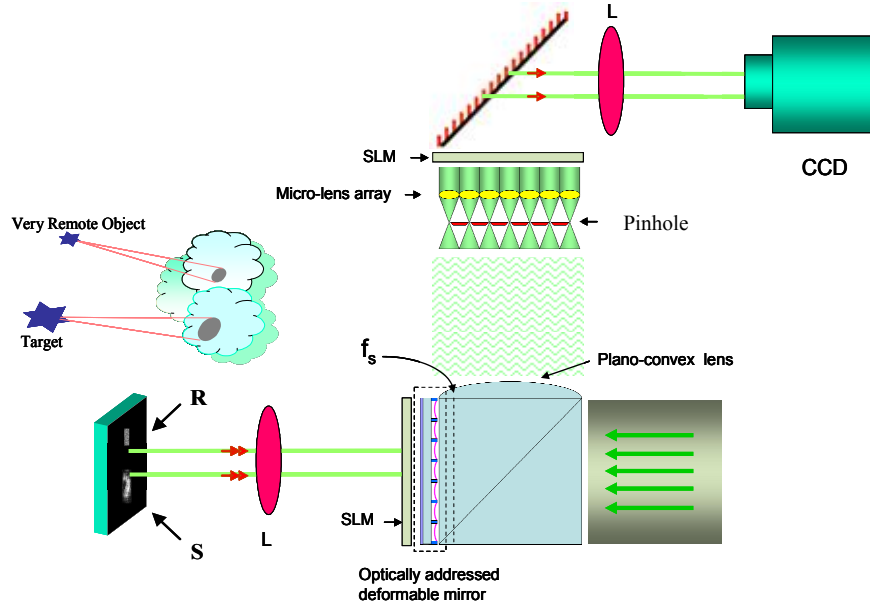


Figure 8. Schematic diagram of a nonlinear optical limiter MEMS joint Fourier processor

The input-output nonlinear transfer function of the NOLMEMS device, which shows the relationship between the light transmitted through the pinhole to the light intensity incident on the back side of the device is given by¹²:

$$G(y) \propto \left(\frac{Ay}{Ay + B} \right)^2 \quad (6)$$

where the parameters are defined as:

$$A = 8\lambda Ts^2 \quad (6a)$$

$$B = r_1^6 V^2 L^2 \omega^2 \pi^3 \epsilon_0^3 \quad (6b)$$

$$y = (a + b(\Delta n + n)^2) \quad (6c)$$

$$a = L^2 \omega^2 \pi^2 r_1^4 \epsilon_0^2 \quad (6d)$$

$$b = q^2 \mu_n^2 A_d^2 s^2 \quad (6e)$$

In the above equations, λ is the back-illumination wavelength, ϵ_0 is permittivity of free space, $2r_1$ is the diameter of a pixel, s is the depth of the well, T is the membrane tension, V is the total voltage applied across the MEMS, q is the electronic charge, μ_n is the carrier mobility, L is substrate thickness, A_d is the area of each pixel, and ω is the angular frequency. n and Δn are the substrate carrier concentration and the photo-generated carrier concentration, respectively.

The effectiveness of the proposed image recovery was tested with computer simulation. A 128×128 pixel Lena face located in the middle of a 512×512 null array was used for the input image. The blurred image was generated by convolving the original input with common blur functions: motion, atmospheric turbulence, and misfocusing. Random noise was also added to the blurred image. The noise was created by a random-number generator that produced white Gaussian noise with zero mean and a variance of 1, and was added to the blurred joint input.

The motion impulse response was a 2×50 pixel rectangle. The atmospheric turbulence was¹⁶:

$$H(v_x, v_y) = e^{-\beta(v_x^2 + v_y^2)^{5/6}} \quad (7)$$

for $\beta=0.0025$. The misfocusing impulse response was a circle of ones with a diameter of 20 pixels.

The nearly hard-clipping nature of the NOLMEMS device saturation nonlinearity fully clips the joint spectra high frequencies, even for low light intensities.

Figure 9 shows the simulation results. Figure 9(A) is the noisy blurred input via motion aberration with SNR= 1 and 9(A') is the corresponding recovered image. Figure 9(B) is the noisy input blurred via atmospheric turbulence with SNR= 1 and 9(B') is the corresponding recovered image. Figure 9(C) is the noisy blurred input via misfocusing aberration with SNR= 1 and 9(C') is the corresponding recovered image.

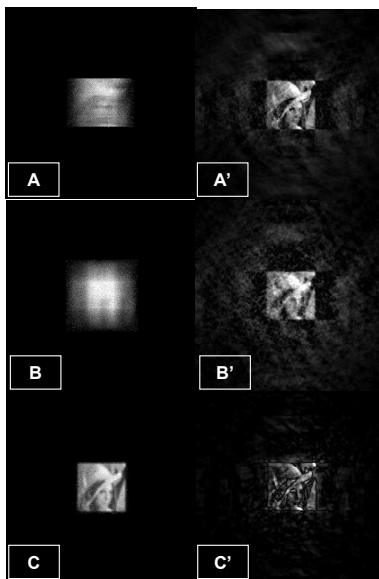


Figure 9. (A) Noisy blurred input via motion aberration with SNR= 1, (A') recovered image, (B) noisy blurred input via atmospheric turbulence with SNR= 1, (B') the corresponding recovered image, (C) noisy blurred input via misfocusing aberration with SNR= 1, and (C') the corresponding recovered image.

It is clear from the simulation results that dynamic range compression deconvolution via NOLMEMS is capable of both noise reduction and image restoration embedded in a severe noise environment from any kind of image aberration. Signal-to-noise ratio of one means that the probability of signal detection is $\sim 50\%$ with 0.1 average false alarm rate (\overline{FAR}).

8. CONCLUSION

This paper proposes dynamic range compression deconvolution using three forms of nonlinearities: (a) digital implementation- A-law/ μ -law, (b) hybrid digital-optical implementation- two beam coupling photorefractive holography, and (c) all optical implementation- MEMS deformable mirrors. Dynamic range compression deconvolution could be used as a preprocessor for enhancing Automatic Target Recognition system performance. We showed that dynamic range compression deconvolution (DRCD) outperforms the best well-established filters in the image processing area, since it has three important functionalities that other approaches do not have:

- (a) DRCD enhances the low frequency intensities relative to the high frequencies
- (b) DRCD enhances the signal to noise ratio (SNR) where the signal spectrum is less than the noise spectrum and reduces the signal to noise ratio where the signal is higher than the noise
- (c) DRCD up converts the low frequencies noise to high frequencies leading to spread the noise over a very broad area and subsequently enhances the SNR. The computer simulation results for all three algorithms outperformed the image restoration via the Wiener filter for images embedded in high noise levels.

REFERENCES

- (1) Larry C. Andrews, "Field Guide to Atmospheric Optics," SPIE field guides, Vol. FG05, John E. Greivenkamp, Series Editor (2004)
- (2) Jed Khoury, Peter D. Gianino, and Charles L. Woods "Companding nonlinear correlators," Proc. SPIE Int. Soc. Opt. Eng. Vol. 5362, 160-177 (2004)
- (3) Jehad Khoury, Mark Cronin-Golomb and Charles L. Woods, "Photorefractive implementations of coherent spatial/temporal signal detection," Proc. SPIE Int. Soc. Opt. Eng. Vol. 2529, 238-249 (1995)
- (4) <http://hyperphysics.phy-astr.gsu.edu/hbase/audio/tape4.html#c2>
- (5) H. Stark, F. B. Tuteur, and J. B. Anderson, Modern Electrical Communication, Analog, Digital and Optical Systems, 2nd ed. (Prentice-Hall, Englewood Cliffs, N.J., 1988), Chap. 4, pp. 175-178; Chap. 6, pp. 247-248.
- (6) John G. Proakis, Masoud Salehi, "Communication Systems Engineering," Prentice Hall (2002)
- (7) Bahareh Haji-saeed; Sandip K. Sengupta; William D. Goodhue; Jed Khoury; Charles L. Woods; John Kierstead "Dynamic range compression deconvolution using A-law and μ -law algorithms", Proceedings Vol. 6574, Optical Pattern Recognition XVIII (2007)
- (8) B. Haji-Saeed, S. K. Sengupta, W. Goodhue, J. Khoury, C. L. Woods and J. Kierstead, "Nonlinear dynamic range compression deconvolution", Optics Letter Vol. 31, 1969-1971 (2006)
- (9) Jed Khoury, Charles L Woods, Bahareh Haji-Saeed, John Kierstead, "Two-beam coupling deconvolution via spatially variable dynamic spectral compression", Proc. SPIE Vol. 5816, p. 277-283, Optical Pattern Recognition XVI (2005)
- (10) Jed Khoury; Charles L. Woods; Bahareh Haji-saeed; Sandip K. Sengupta; William D. Goodhue; John Kierstead, "MEMS deformable mirror optical limiter for dynamic range compression deconvolution", Proceedings Vol. 6556 Micro (MEMS) and Nanotechnologies for Defense and Security (2007)
- (11) B. Haji-saeed, S. K. Sengupta, W.D. Goodhue, J. Khoury and C. L. Woods and J. Kierstead "Dynamic Range Compression Deconvolution based on MEMS Deformable Mirror Optical Limiter", OSA, Rochester, NY (2006)
- (12) Bahareh Haji-saeed, "Development of Novel Device Assemblies and Techniques for Improving Adaptive Optics Imaging Systems", PhD. Thesis Dissertation, University of Massachusetts at Lowell (2006)
- (13) H.J. Eichler, P. Gunter, and D.W. Pohl, "Laser Induced Dynamic Gratings", Springer-Verlag, Berlin (1986)
- (14) T. J. Hall, R. Jaura, L. M. Connors, P. D. Foote., "The photorefractive effect—a review", Prog. in Quant. Elec., Vol. 10, pp. 77-146 (1985)
- (15) P. Gunter and J.-P. Huignard, "Photorefractive materials and their applications", Vol. I & II, New York: Springer Verlag (1988)
- (16) Rafael C. Gonzalez, Richard E. Woods, "Digital Image Processing," Prentice Hall (2002)